JPhys Energy

PAPER • OPEN ACCESS

Origin and avoidance of double peaks in the induced voltage of a thermomagnetic generator for harvesting low-grade waste heat

To cite this article: Daniel Dzekan *et al* 2022 *J. Phys. Energy* **4** 024006

Journal of Physics: Energy

OPEN ACCESS

RECEIVED
22 December 2021

REVISED
28 February 2022

ACCEPTED FOR PUBLICATION
9 March 2022

PUBLISHED
14 April 2022

PAPER

Origin and avoidance of double peaks in the induced voltage of a thermomagnetic generator for harvesting low-grade waste heat

Daniel Dzekan[1,2], Tim D Kischnik[1,3], Anett Diestel[1], Kornelius Nielsch[1,2] and Sebastian Fähler[1,4,*]

[1] Leibniz IFW Dresden, Helmholtzstraße 20, 01069 Dresden, Germany
[2] TU Dresden, Helmholtzstraße 8, 01069 Dresden, Germany
[3] Martin-Anders-Nexö-Gymnasium, Haydnstraße 49, 01309 Dresden, Germany
[4] Helmholtz-Zentrum Dresden-Rossendorf, Bautzner Landstraße 400, 01328 Dresden, Germany
[*] Author to whom any correspondence should be addressed.

E-mail: s.faehler@hzdr.de

Keywords: thermomagnetic energy harvesting, thermomagnetic generator, thermomagnetic material, magnetocaloric material, waste-heat recovery

Abstract

Thermomagnetic harvesting is an emerging approach used to convert low-grade waste heat to electricity, which recently obtained a boost due to the development of both more efficient functional materials and innovative device concepts. Here, we examine a thermomagnetic generator which utilizes gadolinium as the thermomagnetic material and report on the double peaks of the induced voltage. Using a combination of experiments and theory we show that these double peaks originate from the interaction between an asymmetric magnetization curve and a pretzel-like magnetic field topology. Double peaks are detrimental for the output power and can be avoided by matching the magnetization change by adjusting the cold and hot fluid flow.

1. Introduction

The increasing evidence of a human-made climate change [1, 2] underpins the need to use the primary sources of energy as efficiently as possible. This includes recovering waste heat and converting it to electrical energy. However, most of this waste heat is available at temperatures just above ambient [3]—a temperature range where hardly any technology, except thermoelectrics, is available [4]. Thermomagnetic harvesting of low-grade waste heat is an alternative emerging technology [5, 6], which promises to be more energy efficient and affordable in this temperature range [7, 8]. This technology utilizes a thermomagnetic material, which exhibits a steep change in magnetization in the vicinity of the temperature of the available waste heat. Although invented more than a century ago [9, 10], thermomagnetic harvesting obtained a boost [11] after appropriate materials were developed as a side product for magnetocaloric refrigeration, which is the reverse energy conversion process [12, 13]. This illustrates the close connection between novel functional materials and innovative applications—an intimate combination which will be addressed in this paper in more detail.

Three different types of thermomagnetic devices can be identified, depending on their type of movement [8]: rotating thermomagnetic motors, linear oscillators and generators. Thermomagnetic generators (TMG) are the only devices which require no movement, since these devices utilize the steep change in magnetization of a thermomagnetic material to switch the magnetic flux which, according to Faraday's law, induces a voltage peak in a coil wrapped around the material. Recently, we presented a pretzel-like magnetic field topology, which allowed for a flux reversal, which improved the performance of TMGs by orders of magnitude [14]. In this work we will use this particular TMG, and demonstrate that under certain circumstances not a single voltage peak is induced, but double peaks occur, which reduce the efficiency strongly. To understand the physical origin of these unexpected double peaks, we will examine the interaction between the thermomagnetic material and the TMG in detail by experimental and theoretical means.

The performance of a thermomagnetic system is strongly determined by the thermomagnetic material used [8, 15] and many more materials have been suggested recently [16–18]. While most material libraries

are based on literature values of material properties, only a few direct experimental analyses of thermomagnetic materials are available [19]. For the particular TMG used here, we recently published a comparison between La–Fe–Co–Si and Gd [20]. Although Gd exhibited an inferior performance, we selected this thermomagnetic material for the present experiments as it is the reference material used for most previous thermomagnetic devices [21–24]—and it is still the benchmark magnetocaloric material [25, 26]. Furthermore, Gd exhibits a typical second-order Curie transition, which results in an asymmetric magnetization vs temperature $M(T)$ curve, which is the more general case compared to La–Fe–Co–Si that has a close to first-order transition. The need for more detailed experiments is evidenced by the fact that, until now, double peaks within a TMG have been neither reported nor predicted.

To understand the origin and to finally eliminate the double peaks within a TMG, this paper is organized as follows. After a short description of the TMG used in section 2, in section 3 we systematically analyze the experimental conditions, which result in the formation of double peaks. We focus on the influence of the fluid flow, since this can easily be varied independently for the hot and cold fluids. As this controls the heat exchange, this allows us to adjust the magnetization change, which depends on both temperature and time $M[T(t)]$. To disentangle the contribution of the cold and hot sides, we additionally analyze experiments where only one side of the TMG is filled with thermomagnetic material. To demonstrate the detrimental impact of double peaks on the power output, we systematically vary the flow rates of both fluids and cycle frequency. In section 4 we present a model, which describes the temperature and time dependency of the flux change on both sides. We intentionally selected a quite simple semi-analytical model as, in contrast to a fully numerical model, this clearly allows us to attribute the origin of double peaks to the different $M[T(t)]$ dependencies of the hot and cold sides. Our analysis reveals that double peaks originate from the combination of the asymmetric magnetization curve $M(T)$ of Gd and the particular pretzel-like magnetic field topology, which enables flux reversal. We demonstrate that the use of different fluid flow rates allows us to match the magnetization change in both sides in time, which increases the power output of a TMG by avoiding double peaks and unfavorable magnetic stray fields.

2. Materials and methods

In this work we examine the coupled behavior of magnetization change and heat transfer on the induced voltage in a TMG. As a generator (figure 1), we use a recently developed prototype with an advanced magnetic flux topology [14]. In the TMG two Nd–Fe–B permanent magnets (VACODYM 722, VACUUMSCHMELZE) generate a magnetic flux Φ. This magnetic flux is guided within two identical magnetic circuits. Each circuit consist of two iron yokes and a thermomagnetic material, which is arranged as a set of 25 Gd plates with a thickness of 0.5 mm [20]. Around the magnetic circuit a mixing chamber is constructed with two entrance and two exit hose connections for the heat exchange fluid. The two magnetic circuits are connected by two steel cores surrounded by copper coils , each with 1000 turns.

During the operation of the TMG, cold and hot fluids (water with 40% propandiol) are pumped inside the mixing chambers. The temperature control and the pumping of the fluid is provided by two thermostats (CBC 5 control, IKA). Four three-way valves guide the cold fluid in one chamber and hot fluid in the other, which is alternated after 5 s. The temperature of the fluid is measured by Pt1000 thermoresistors directly before the entrance and after the exit. While the fluid moves through the fluid channel between the Gd plates (with the same thickness as the plates), it exchanges heat with the thermomagnetic material. In one magnetic circuit the thermomagnetic material is cold, while it is hot in the other circuit. In the cold state, with temperatures below the Curie temperature, Gd has high magnetization. Hence, the magnetic resistivity of the material is low, which means that it has a high conductivity for the magnetic flux. On the other site, Gd has low magnetization for temperatures higher than the Curie temperature. In the low magnetization state the magnetic flux cannot be guided by the material. As the two magnetic circuits are connected, the magnetic flux of both permanent magnets close over the side with the cold Gd. When using an electric circuit, as an analogy, the thermomagnetic material can be considered as a magnetic switch, which is closed when the material is cold and open at higher temperatures. When the valves get activated, hot and cold fluids switch sides and the temperature of the thermomagnetic material. With that, the previously open switch is closed and the previously closed switch becomes open. Accordingly, the magnetic flux of the permanent magnets changes its direction and now closes over the other side. Due to Faraday's law of induction (equation (1)), this change in magnetic flux inside the iron cores, which connect both magnetic circuits, results in an induced voltage in the copper coils:

$$V_{\mathrm{ind}} = -N\frac{\mathrm{d}\Phi}{\mathrm{d}t}. \tag{1}$$

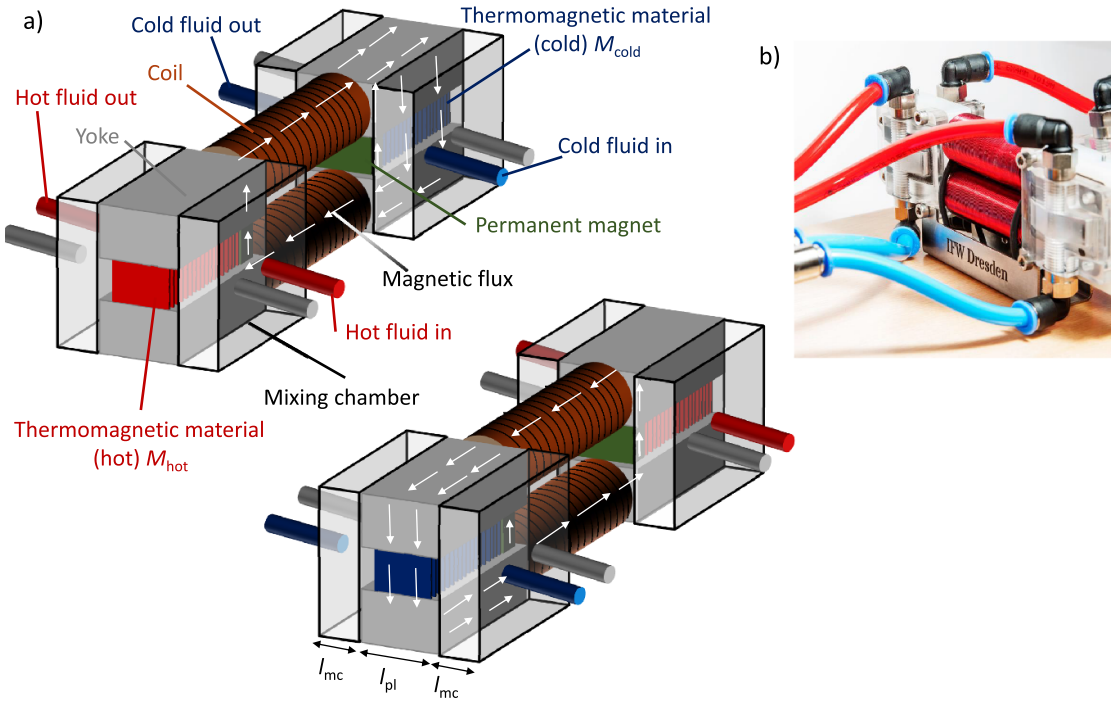

Figure 1. The TMG, which allows for a magnetic flux reversal due to it pretzel-like magnetic circuit design [14]. (a) Two schematic views of the TMG illustrate all the components of the device and its working principle. The magnetic flux Φ is provided by two permanent magnets and is guided over a yoke to the thermomagnetic material, arranged as 25 Gd plates. One side of the generator is cooled down, while the other is heated up, due to hot and cold fluid going into the mixing chamber (length l_{mc}) and traveling across the plates (length l_{pl}). The magnetic flux is then closed over the cold material since it has high magnetization, M_{cold}, while the hot material has low magnetization, M_{hot}. Alternating the cold and hot fluid with three-way valves switches the magnetic flux direction. Accordingly, a voltage is induced within the induction coils. (b) A photograph of the TMG with the pretzel-like magnetic circuit design. Reprinted with permission from Springer Nature Customer Service Centre GmbH: Springer Nature, Nature Energy [14] © 2019.

Here, the coil winding number N connects the induced voltage V_{ind} with the time-dependent change in the magnetic flux. This flux change is determined by the change in magnetization inside the material. Thereby, the magnetization change itself depends on the time-dependent temperature change. In an ideal case the thermomagnetic material acts as a flux switch, which is open (no flux guidance at all) in the hot state and closed for the cold state, where the total magnetic flux can be guided inside the material. Thus, the temperature-dependent magnetization change and the time-dependent temperature change are maximal, resulting in an infinite induced voltage. However, in the real case the magnetization increases or decreases continuously over the temperature span, and it also takes some time to change the temperature. With this, the induced voltage is reduced compared to the ideal case. This particular TMG design minimizes magnetic stray fields and, therefore, reaches the highest performance of all the TMGs today [14]. In this paper we consider a consequence of this design, which is the need for a simultaneous flux change on both sides. This means that the decrease of the magnetic flux change during heating has to be compensated by the magnetic flux increase by cooling. Accordingly, it is necessary to match the magnetization change and the heating and cooling rates, respectively. These aspects are analyzed experimentally in the next section and theoretically in section 4.

3. Experimental results

The induced voltage in the TMG is a combination of temperature-dependent magnetization change and time-dependent temperature change. As the change in magnetization with temperature is a material property, it is fixed for a certain temperature difference ΔT. Therefore, the only way to influence the induced voltage at a constant ΔT (and a fixed middle temperature T_{middle}) is to change the heat exchange of the fluid with the thermomagnetic plates. Since the thermal diffusivity is also a material property, heat exchange by conduction in a given design only depends on the properties of the thermomagnetic material, which is Gd in this work. With this, the only way to affect the heat transfer and thus the induced voltage is by varying the fluid flow. Thereby, the heat can be brought to the thermomagnetic material faster and the temperature changes faster. In our setup we can change the flow rate of hot and cold fluids independently by setting the rounds per minute of the pumps in the thermostats. Accordingly, it is possible to investigate the influence of different flow rates on the induced voltage.

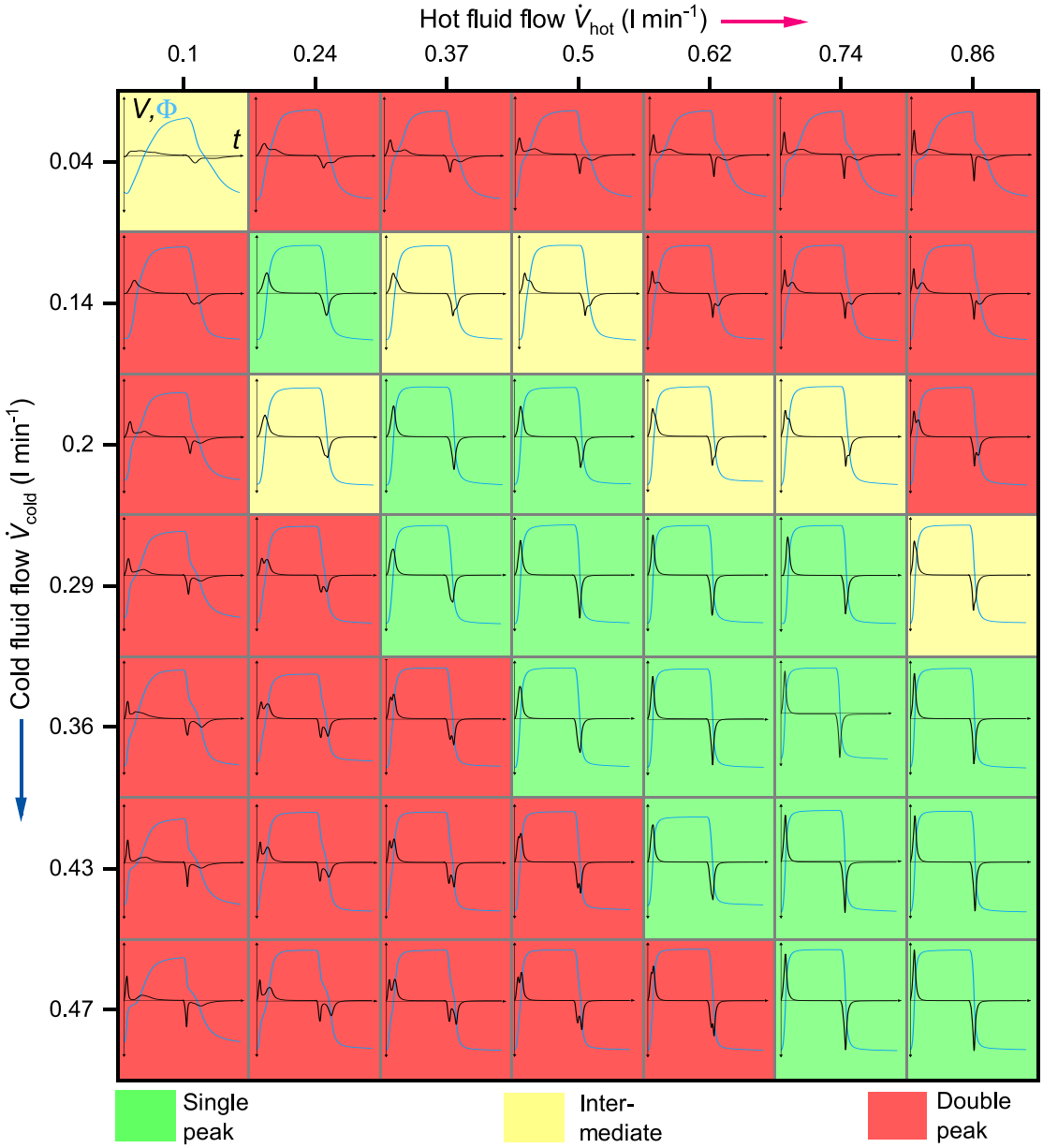

Figure 2. Voltage and magnetic flux profiles as a result of the heat exchange fluid flow rate at a temperature difference of 30 K. After alternating the temperature we only observe a single voltage peak (green background color), if the hot fluid rate is roughly twice as high as the cold fluid rate. Otherwise, a second peak immediately follows the first induction peak (red) or an intermediate voltage profile appears (yellow). To understand the unexpected double peaks, this paper examines in depth the influence of hot and cold fluid flow when using thermomagnetic materials with an asymmetric magnetization curve. The *x*-axis of each box represents a span of 10 s, which is required for a complete cycle at 0.1 Hz. The *y*-axis represents the voltage V (black, in the range of −0.1 to 0.1 V) and the magnetic flux change Φ (blue, in the range of -8×10^{-6} to 8×10^{-6} Wb), respectively. All measurements are performed under open circuit conditions.

In figure 2 we summarize the open circuit voltage (no current flow) profiles (black curves) and the integrated magnetic flux change (blue curves) for different fluid flow rates of hot V_{hot} and cold V_{cold} fluid at $\Delta T = 30$ K and $T_{middle} = 292$ K. Thereby, the hot fluid rate varies from 0.1 l min^{-1} up to 0.86 l min^{-1}. For the cold fluid the maximal reachable flow rate is limited to 0.47 l min^{-1}. This limitation results from the exponential increase in viscosity within the heat exchange fluid at lower temperatures. Therefore, at the highest pressure of the pumps in the thermostats, the maximal flow rates are different for hot and cold fluids. From previous results with a La–Fe–Co–Si alloy as the active material, we expect, at a frequency of 0.1 Hz, a voltage profile with two sharp peaks in a time span of 10 s [14]. However, using Gd plates as the thermomagnetic material, we observe different appearances for the induced voltage profiles, depending on the flow rates. Indeed, we observe three different types of voltage peaks: first, the expected single peak, which occurs every time after the valves have switched. The second type is a voltage peak followed by a lower or higher second peak, which we will call in the following a double peak. The third appearance is in between the

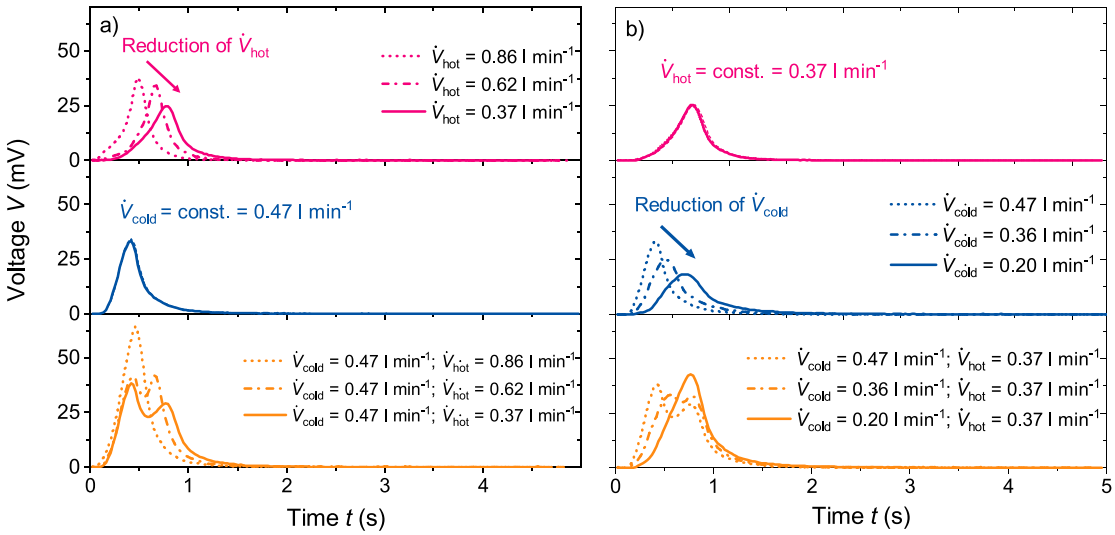

Figure 3. Measurement of open circuit voltage for different fluid rates after the first five seconds after switching. Here, only one side of the TMG is filled with Gd plates. With this, the active material is heated up after the first switching event and cooled down after the second switching event. Thereby, it is possible to distinguish between the induced voltage due to heating (red) and cooling (blue). By adding these voltages up (orange), it is possible to draw conclusions on the complete voltage when both sides are filled with Gd plates. (a) At a constant flow rate of cold fluid $\dot{V}_{cold} = 0.47\,\mathrm{l\,min^{-1}}$, the hot flow rate is decreased from $\dot{V}_{hot} = 0.86\,\mathrm{l\,min^{-1}}$ down to $\dot{V}_{hot} = 0.37\,\mathrm{l\,min^{-1}}$. This represents the lowest row of figure 2. As a result the voltage peak occurs at a late time and with a lower maximum. Accordingly, the voltage peak leads to an offset between cooling and heating and a double peak in the voltage summer. (b) Reducing the cold flow rate at a constant hot flow rate $\dot{V}_{hot} = 0.37\,\mathrm{l\,min^{-1}}$ (third row of figure 2) reduces the induced voltage during cooling and shifts the maximum to a longer time, at which the voltage for heating also peaks. Accordingly, the summation of both voltages results in a single peak voltage characteristic.

two previous cases: not a clear single peak but a peak with a following shoulder. To distinguish the different cases we mark, in figure 2, those conditions resulting in a single peak, double peaks and intermediate cases with green, red and yellow background colors, respectively.

In the measurement matrix of figure 2 both fluid flow rates are minimal in the top left corner. For this condition the induced voltage is very small due to a long time over which the induction takes place. In fact, it is longer than the switching period time of 5 s, which indicates an incomplete heat exchange and, as result, a reduced magnetic flux change compared to the other measurements. The induced voltage increases when increasing the flow rates. However, we observe a single peak only when the hot flow rate is around twice as high as the cold flow rate. In the diagram these conditions are in the diagonal direction from the upper left to the lower right. When we increase only one flow rate, starting at the conditions $V_{hot} = 0.37\,\mathrm{l\,min^{-1}}$ and $V_{cold} = 0.20\,\mathrm{l\,min^{-1}}$, we observe a change in appearance of the voltage profile. This is followed by a reduction in the maximum induced voltage and a broader width of the peaks. A clear double peak is formed when we increase the cold flow rate, while a higher hot flow rate results in an intermediate peak. Accordingly, we observe a strong influence of the flow rates on the induced voltage.

Although we recognize that the voltage profile is affected by the ratio of the cold and hot fluid rates, it is difficult to distinguish the influence of one of these processes on the induced voltage. This is attributed to the generator design, where the switching of the valves starts the heating of one side simultaneously with cooling of the other side. Therefore, the measured voltage is affected by any kind of magnetic flux change. To separate the impact of heating and cooling, respectively, on the induced voltage we removed the Gd plates of one side. By doing so, the first heat exchange process after switching is linked to heating and the second heat exchange process to cooling. The addition of both absolute induced voltages allows us then to draw conclusions on the complete voltage when both sides are filled with Gd plates. Accordingly, with this approach it is possible to separate the consequences of different flow rates on the appearance of the voltage peak.

In figure 3 we display the induced voltage separately for the heating and cooling scenarios when only one side of the TMG is filled with Gd plates. We focus on two different scenarios. First (figure 3(a)), we measure the induced voltage for $0.47\,\mathrm{l\,min^{-1}}$ and $V_{hot} = 0.86\,\mathrm{l\,min^{-1}}$. Both voltage peaks have nearly the same height for heating and cooling and occur at the same time, just before 0.5 s. As a result, the sum of both, represented by the orange dotted line, results in a single peak. This is nearly identical to the peak appearance in figure 2 under equal conditions, where both sides are filled with plates. When we decrease the hot flow rate the voltage induced by heating also decreases and peaks later than 0.5 s. Now, this shift results in a double peak when we add up both individual voltages (orange dashed curve). The second peak is higher than the first, as

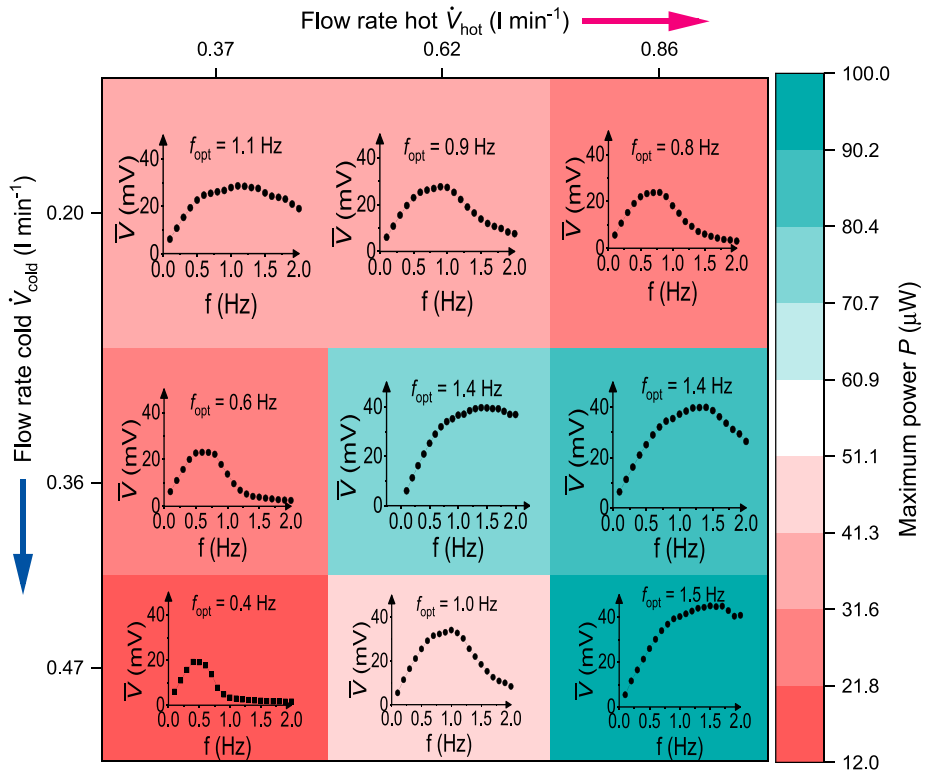

Figure 4. Average voltage and power output as a result of cold and hot fluid flow rates. The heat map represents the generated power P within the TMG for different fluid flow rates. The power increases from the upper left corner, where the fluid flow is low, $\dot{V}_{cold} = 0.2\,\mathrm{l\,min^{-1}}$ and $\dot{V}_{hot} = 0.37\,\mathrm{l\,min^{-1}}$ to the lower right, where both fluid rates are maximal ($\dot{V}_{cold} = 0.47\,\mathrm{l\,min^{-1}}$ and $\dot{V}_{hot} = 0.86\,\mathrm{l\,min^{-1}}$). This increase in output power results from a higher optimal cycle frequency f_{opt} and average induced voltage $\overline{V}$ due to a faster heat exchange. The average induced voltage per cycle frequency is shown in the inserted graphs. If just the cold or hot fluid rate is increased based on the upper left conditions, the optimal cycle frequency and maximum output power decrease, despite higher input power.

measured in figure 2. A further decrease in the hot flow rate shifts the voltage peak as a result of heating to even longer times with a reduced maximum voltage. As a consequence, the sum (orange solid line) indicates a double peak with a broader width and a lower second peak.

In the second scenario (figure 3(b)) we keep the hot flow rate $V_{hot} = 0.37\,\mathrm{l\,min^{-1}}$ constant and only vary the cold flow rate. For this hot flow rate, the induced voltage due to heating has a maximum of 25 mV, which occurs between 0.5 s and 1 s. Much earlier, namely just before 0.5 s, the higher voltage as a result of cooling occurs for $V_{cold} = 0.47\,\mathrm{l\,min^{-1}}$. The addition of both voltages (orange dotted curve) results in a double peak, as in figure 3(a), under identical conditions. Now, we decrease the cold flow rate down to $0.36\,\mathrm{l\,min^{-1}}$ so that both flow rates are the same. Thereby, the induced voltage due to cooling decreases and the maximum shifts to around 0.5 s. This shift reduces the double peak characteristics in the voltage addition, represented by the orange dashed line, as also measured in figure 2. However, the double peak in the voltage profile only disappears if we reduce the cold flow rate further to $0.2\,\mathrm{l\,min^{-1}}$. Accordingly, for both scenarios we only observe a single peak, when the hot flow rate is twice as high as the cold flow rate. For these conditions only, the induced voltage contributions by both heat exchange processes—heating and cooling—have their maximum at the same time.

In the following, we ask if the different features of the measured voltage profiles have an direct impact on the TMG performance. For this we measure, in figure 4, the power output with Gd plates on both sides again, depending on the hot and cold flow rates. We measure the power of the TMG with $P = \frac{|\overline{V}|^2}{R}$, whereby $|\overline{V}|$ is the average induced voltage per cycle and R is the load resistance. We set a load resistance of $R = 9.15\,\Omega$, resulting in the maximal power [14]. Inside each field of the heat map we show the average induced voltage depending on the cycle frequency. For $V_{hot} = 0.37\,\mathrm{l\,min^{-1}}$ and $V_{cold} = 0.20\,\mathrm{l\,min^{-1}}$ the average induced voltage is maximal at an optimal cycle frequency $f_{opt} = 1.1$ Hz, resulting in a output power of 45 μW. In figures 2 and 3 we observe a single peak at these flow rates. Increasing both flow rates results in a higher output power up to 95 μW, since the optimal frequency ($f_{opt} = 1.5$ Hz) and thus the average voltage can be higher. However, this is only the case if we increase the hot and cold flow rates in such a way that only a single peak occurs. For conditions where only one flow rate is increased (e.g. $V_{hot} = 0.86\,\mathrm{l\,min^{-1}}$ and

$V_{cold} = 0.20\,\mathrm{l\,min^{-1}}$) and the voltage profile has a double peak characteristic, the output power decreases. This reduction results from the lower optimal frequency and thus average voltage. Indeed, f_{opt} decreases to 0.4 Hz for $V_{hot} = 0.37\,\mathrm{l\,min^{-1}}$ and $V_{cold} = 0.47\,\mathrm{l\,min^{-1}}$, although the cold flow rate is higher compared to the upper left conditions. Consequently, in this case, the output power of the TMG is lower, although the input energy is higher. This is a key issue, since it shows that maximum fluid flow does not automatically result in higher performance. Only under those conditions where the voltage profile has a single peak is the thermal input energy efficiently converted into electric energy.

4. Theoretical considerations

In the experimental section we observed different appearances of the induced voltage profiles. Three types of voltage peaks occur, depending on the hot and cold fluid flow rates. As the different voltage profiles influence the optimal cycle frequency and thus the output power, it is important to understand why different voltage profiles are formed. To describe the different shapes of voltage peaks we present a simplified model in the following. With this model it is also possible to predict the best operating conditions for different thermomagnetic materials to achieve a single peak voltage profile and the maximal power output.

To describe the induced voltage in the TMG we have to look at the magnetic flux inside the magnetic circuit. The magnetic flux depends on the magnetization M of the thermomagnetic material and the applied magnetic field H from the permanent magnets:

$$\Phi = \frac{\mu_0 (M + H)}{A}. \tag{2}$$

Here, μ_0 is the induction constant and A is the surface area of the magnetic circuit component through which the magnetic flux closes. In this equation the magnetization is the key material property, as its temperature dependence results in the switching of the magnetic flux in the TMG. As, in this particular generator design, the magnetic flux is always guided inside the magnetic circuit of any of the two sides, it is possible to approximate the upper limit of the magnetic flux change using the magnetization change of the thermomagnetic material. Therefore, we can also approximate the induced voltage as follows:

$$V_{ind} \approx -N \cdot \mu_0 \cdot A \cdot \frac{\mathrm{d}M}{\mathrm{d}t}. \tag{3}$$

Therefore, the induced voltage depends on the time-dependent change in magnetization. As the magnetization of the material depends on the temperature, the time-dependent characteristics are determined by the temperature change in the material as a result of heating and cooling of the material. As a consequence, the magnetization is a function of the temperature, which itself is a function of time $M = f[T(t)]$. Using the chain rule of differentiation, we can unbundle the time-dependent change in magnetization in two parts. As evident from equation (4), we have to consider both the temperature-dependent change in magnetization and the time-dependent temperature change:

$$\frac{\mathrm{d}M}{\mathrm{d}t} = \frac{\mathrm{d}M}{\mathrm{d}T} \cdot \frac{\mathrm{d}T}{\mathrm{d}t}. \tag{4}$$

The induced voltage is thus a linked connection of the temperature-dependent change in magnetization and the time-dependent temperature change. In the following we now look closer at both terms of the equation separately. For the first term we measure the magnetization of the thermomagnetic material (Gd) with regard to dependence of the temperature, as shown in figure 5. Accordingly, we can calculate the temperature-dependent magnetization change $\frac{\mathrm{d}M}{\mathrm{d}T}$, which differs for the cooling and heating side. When considering the cold material during heating, it loses its magnetization and, accordingly, $\frac{\mathrm{d}M}{\mathrm{d}T}$ is negative. The largest change in magnetization occurs close to its Curie temperature, where $\frac{\mathrm{d}M}{\mathrm{d}T}$ exhibits its minimum. On the other hot side the material becomes ferromagnetic, and thus $\frac{\mathrm{d}M}{\mathrm{d}T}$ is positive and a maximum is observed.

As a consequence, the increase in magnetization during the cooling of one side is not always balanced by a decrease during heating on the other side. For example, at the beginning of the temperature change the magnetization of the heated material decreases faster than the magnetization of the cooled material increases, whereas it is the opposite at the end of the temperature change. To describe the influence of this unbalance on the induced voltage we fit the magnetization derivation for heating and cooling (dashed lines). With this fit function (Gaussian plus a linear function) it is possible to link the temperature-dependent magnetization change with the time-dependent temperature change to calculate the induced voltage.

The temperature change with time is the second term of equation (4) and is the more difficult part when describing the time-dependent magnetization change. As we do not have experimental in operando data and

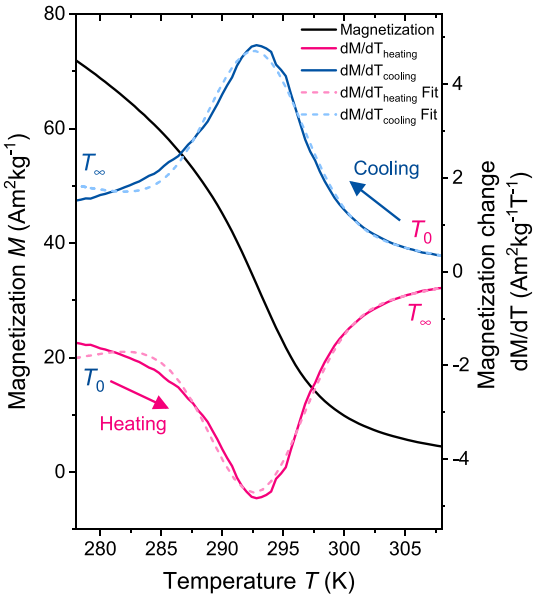

Figure 5. The temperature-dependent magnetization curve of Gd (black line), its derivation as a result of heating (red curve) and cooling (blue curve) for a temperature span of 30 K and the corresponding fit functions (dashed curves). In the TMG the cold material is heated up, while the hot material is cooled down, from the initial temperature T_0 until the end temperature T_∞. Thereby, the material goes from a high magnetic state M_{cold} to a low magnetic state M_{hot} and back. The change in magnetization results in a change in magnetic flux and thus in an induced voltage. The arrows indicate the direction of the heating and cooling process. The measurement is performed in a constant magnetic field of 0.1 T.

an analytical description of the heat exchange is quite difficult, we use a very simple model. In this simplification the temperature change is only determined by the position of the hot and cold fluids within the TMG. This means that when the fluid fronts reach a certain part of the plates it immediately changes the temperature. We consider this simplification justified, as we had previously shown that the heat exchange between the fluid and plates is about five times faster than the time required for the fluid to travel through this TMG [14]. After a certain time, which depends on the fluid flow and respectively velocity, the fluid front reaches the end parts. Subsequently, the material changes its temperature completely and remains at its end temperature for the rest of the cycle. Accordingly, we can describe the temperature of the plates with regard to the dependence on time, as illustrated in figure 6(b), using three different time sections:

$$T = \begin{cases} T_0 & \text{if } t \leqslant t_{mc} = \frac{l_{mc} \cdot A_{mc}}{\dot{V}} \\ T_0 \pm \frac{\Delta T \cdot \dot{V}}{l_{pl} \cdot A_{pl}} \cdot t & \text{if } t_{mc} < t < \left(t_{mc} + t_{pl} = \frac{l_{mc} \cdot A_{mc}}{\dot{V}} + \frac{l_{pl} \cdot A_{pl}}{\dot{V}} \right) \\ T_\infty & \text{if } t > t_{mc} + t_{pl} \end{cases}.$$

In the first time section the temperature T is equal to the initial temperature T_0. The duration t of this section is defined as the time t_{mc}, which the fluid needs to go through the mixing chamber. This time is described by the length l_{mc} and the cross sectional area A_{mc} of the mixing chamber as well as the fluid flow $\dot{V}$. After the fluid front passes the mixing chamber the second time section starts. During this time, the initial temperature decreases or increases—depending on whether we consider the cooling or heating process. The temperature in this section changes in a linear manner with time, whereby the slope is the ratio of the temperature difference ΔT between the cold and hot state (here, $\Delta T = 30$ K) and the time t_{pl} the fluid needs to reach the end of the thermomagnetic plates. This duration is determined by the fluid flow $\dot{V}$, the length of the fluid channels l_{pl} and the total cross sectional area of all the fluid channels A_{pl}. Since the latter are constant in the given device, the slope of the temperature profile and thus the temperature change rate only depends on the fluid flow at a given ΔT.

The magnetization of the first parts of the thermomagnetic material changes as its temperature changes due to the passing fluid. Accordingly, the magnetic flux starts to change and thus the induction of voltage starts. However, the last sections of the plates still remain at their initial temperature, and therefore they do not contribute to the flux change and voltage induction. Hence, it is convenient to divide the thermomagnetic plates section into ten discrete space parts, as illustrated in figure 6(a) (p1–p10). As we obtained the same results with only five discrete parts, we consider ten parts more than sufficient. In each of the separate parts $l_{pl,i}$ we then calculate the individual temperature profile. In the ensuing set of curves, the individual curves are shifted by the time it takes for the fluid to reach the next section. From these curves we

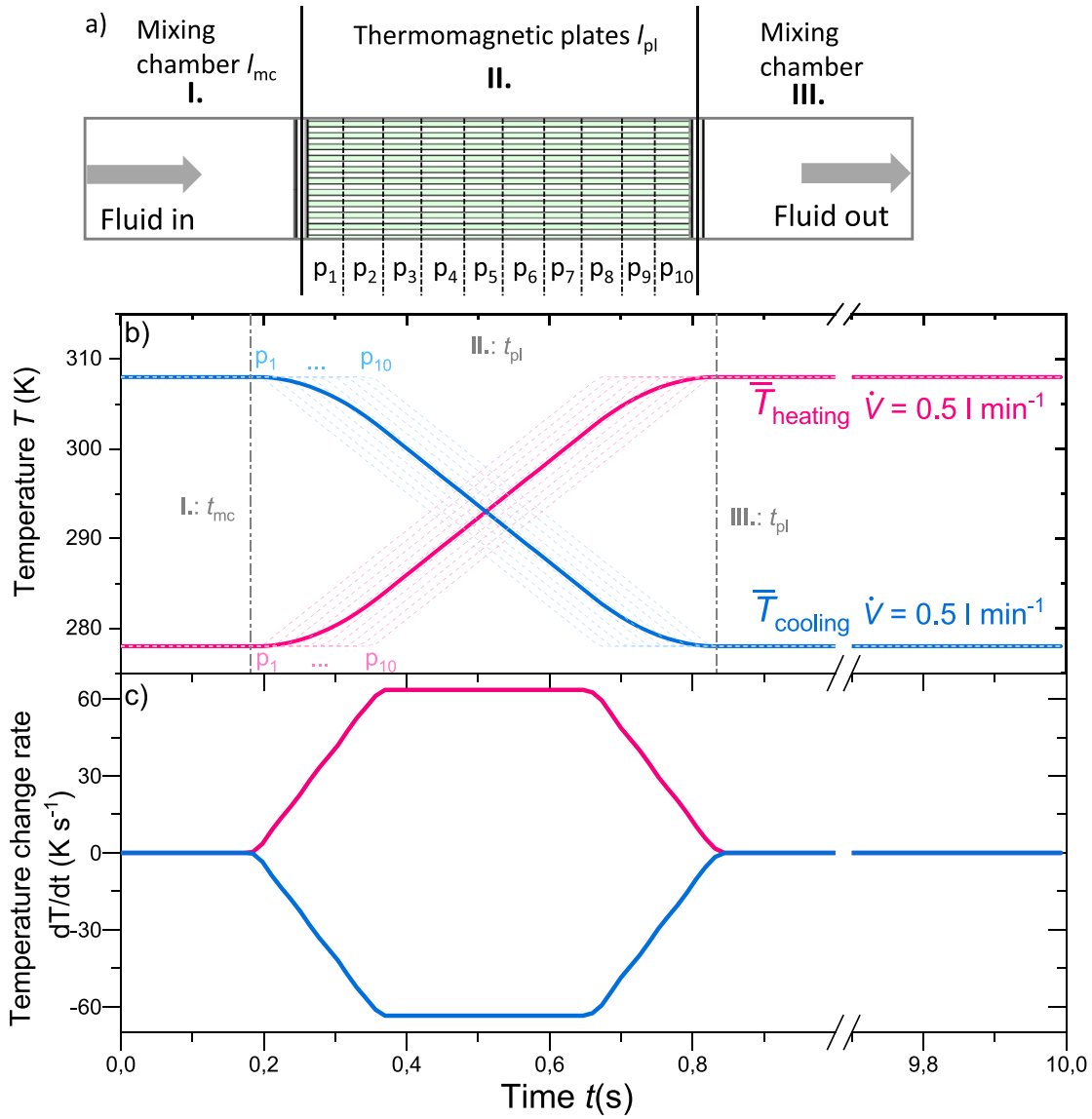

Figure 6. The progression of the calculated material temperature (solid blue and red curves) from the initial T_0 to the end temperature T_∞ and its derivation (dashed blue and red curves) for a temperature span of 30 K. At the beginning, the valves switch and guide the fluids in the opposite mixing chamber. Thereby, the heating and cooling process starts. In the early stages, the temperature changes very quickly. As a consequence, the cooling and heating rates are very high. For longer times these rates decrease and approach zero, as the final end temperature is nearly reached. These calculations are performed for the same flow rates of cold and hot fluid (l min^{-1}).

calculate the mean value, as illustrated in equation (5). With this mean value we can calculate the overall middle temperature $\overline{T}(t)$ of the thermomagnetic material:

$$\overline{T} = T_0 \pm \frac{1}{10}\sum_{i=1}^{10} \frac{\Delta T \cdot \dot{V}}{l_{\mathrm{pl},i} \cdot A_{\mathrm{pl}}} \cdot t. \tag{5}$$

After the fluid passes the last part of the plates, the last time section ($t > t_{mc} + t_{pl}$) starts, in which the average temperature of the material corresponds to the end temperature T_∞.

From the resulting temperature profiles for the cooling and heating process we now calculate the temperature change rate $\dot{T}$ by numerical derivation (figure 6(c)). Hence, we have both terms required for equation (4) and can calculate the time-dependent magnetization change and thus the induced voltage using equation (3).

In figure 7 the calculated induced voltage is shown separately for the cooling and heating process. Adding these voltages results in the total induced voltage as both processes happen simultaneously in our TMG. This procedure is similar to the experimental results shown in figure 3. In these experiments we measure the voltage in the generator for only one side filled with thermomagnetic plates, which allows us to distinguish

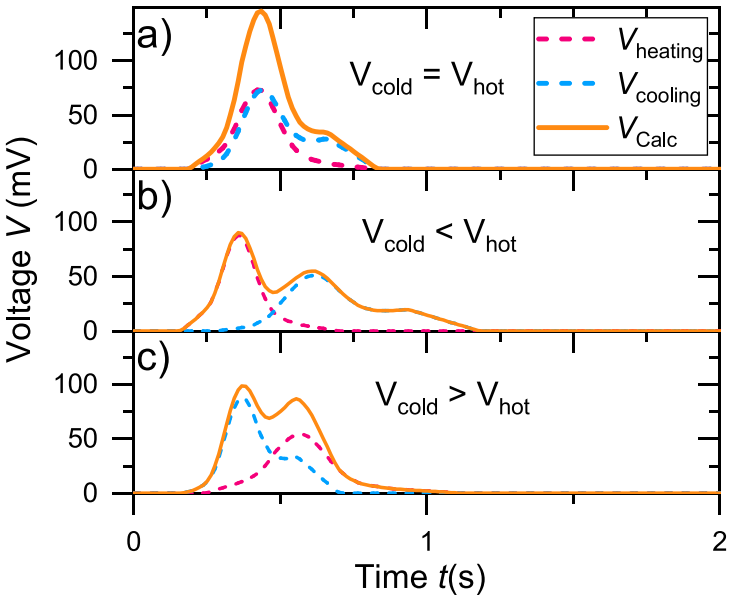

Figure 7. Calculated voltages for three different fluid flow ratios. With the temperature-dependent magnetization change and the time-dependent temperature change we can calculate the induced voltage in the generator using equation (3). This allows a comparison between the calculated voltage and the experimental measured voltage from figures 2 and 3. (a) For the same cold and hot fluid flows ($\dot{V}_{\mathrm{cold}} = \dot{V}_{\mathrm{hot}} = 0.5\,\mathrm{l\,min^{-1}}$) the calculated voltage due to heating has its maximum nearly at the same time as the voltage contribution from the cooling process. However, both curves are not identical, which is particularly true for the decaying curves as a consequence of different magnetization changes for the heating and cooling scenarios. This difference in the voltage due to heating and cooling results in different complete voltages for $\dot{V}_{\mathrm{cold}} < \dot{V}_{\mathrm{hot}}$ (b) and $\dot{V}_{\mathrm{cold}} > \dot{V}_{\mathrm{hot}}$ (c).

between the cooling and heating contribution to the measured voltage. In these experiments the fluid flow is the only operational parameter that has an impact on the induced voltage at a certain temperature difference. Therefore, in figure 7, for the calculated voltage, we consider three cases with different flow rates as well. Hence, we can directly compare the experimental results with the calculations. Although it is not possible to reproduce the experimental values exactly with our simple model, we can clearly see the same behavior of the induced voltage with respect to the fluid flow rates.

In the first case (figure 7(a)) we consider the same fluid flow for the cold and hot fluid. Thus, we obtain the same temperature profile, and respectively its change, for both processes. However, because of the difference in the temperature-dependent magnetization change (figure 5) the calculated voltage due to cooling is not the same as that for the heating process. As a result of the smaller magnetization change in the early stage of the cooling process the induced voltage is lower compared to the voltage induced in the beginning of the heating process. The main difference occurs after the maximum voltage, where the voltage caused by heating decreases significantly faster than that caused by cooling. Although this does not have a major impact on the total voltage for the same fluid flow, this difference becomes quite important for unequal fluid rates. When the hot fluid flow is higher than the cold one (figure 7(b)), the temperature change rate is higher for the heating process and the induced voltage as a result of this process peaks before 0.5 s. In comparison, the induced voltage due to cooling is shifted to longer times and accordingly only reaches lower voltage values. As a consequence, the sum of both voltages results in a first relatively sharp peak, and a second lower but broader peak. Indeed, this is similar to what we observe in our experiments in figure 2 or 3, when the hot fluid flow is much higher than the cold one (for example at $\dot{V}_{\mathrm{hot}} = 0.62\,\mathrm{l\,min^{-1}}$ and $\dot{V}_{\mathrm{cold}} = 0.14\,\mathrm{l\,min^{-1}}$). Next, we consider a larger cold fluid flow (figure 7(c)). Now, the voltage due to cooling is induced faster. However, the voltage due to heating now peaks now on the flank of the cooling voltage. Accordingly, the summed up curve has a different appearance than in the previous case and the second peak has a similar height and width as the first. In the experiments we also find this behavior also in conditions where the cold fluid flow is larger or at least similar to the hot fluid flow.

To summarize this section, the combination of magnetization measurements and a simple model for estimating the temperature profiles in the thermomagnetic materials within the TMG gives an explanation for the three voltage peak appearances observed in our experiments. We can show that different temperature change rates for the heating and cooling processes induce double peaks. Two types of double peaks occur, depending on whether cooling or heating happens faster, since the magnetization changes for both processes are different.

In our experiments we also observed a double peak forming when cold and hot fluids have the same flow rates. We could not reproduce this with our simple model as we did not include the impact of the different fluid properties on the heat exchange. For this we propose to use finite element calculations for computational fluid dynamics in future. However, this simple model presented here already helps to avoid a double peak voltage profile and thus a reduced performance.

5. Conclusion

In this work we investigate different voltage profiles in a TMG for converting low-grade waste heat into electricity with Gd as the thermomagnetic material. In particular, the novel generator design with magnetic flux reversal used in this work has a high potential to become competitive with other low-grade energy harvesting devices. During experimental investigation on this novel prototype we observed three different voltage profileswith regard to the dependency of the flow of the cold and hot heat exchange fluid. To examine the contributions of the heating and cooling processes to the induced voltage separately we changed our setup in such a way that only one side of the generator was filled with thermomagnetic material. Thereby, we observed different voltage profiles for heating and cooling, which resulted in the different appearances of the measured voltage peaks. We observed a direct impact of the voltage profiles on the optimal cycle frequency and thus on the maximum output power of the generator. The highest cycle frequency and power were only obtained for conditions where the hot fluid flow rates were twice as high as those for the cold fluid.

To explain the voltage peaks that formed we describe the magnetic flux change and the induced voltage using a simple theoretical model, which considers both the temperature-dependent magnetization change in the thermomagnetic material and the time-dependent temperature change. We obtained the first factor from magnetization measurements of Gd. For the second factor we developed a simple model, where the temperature change rate only depends on the fluid flow. Indeed, with this we can explain the different voltage peaks and also give predictions for the best operating parameters. Furthermore, we found that in the experiments with the same fluid flows, the heat exchange is different for cold and hot fluids, which can be related to the temperature-dependent fluid properties.

With our combined experimental and theoretical investigation on the different voltage profiles in the TMG with flux reversal we obtained a more precise understanding of the operation of this novel and promising TMG design. Its device performance is intimately connected with the magnetic properties of the thermomagnetic material used and the operational parameters. Our example illustrates that, for the application of novel functional materials, it is essential to understand the interactions of the device and the thermomagnetic material.

As a TMG is most suitable for harvesting low-grade waste heat, large-scale systems may be used for power plants, where most of the energy in this temperature range is wasted. However, it will be some time before reliable systems at this scale will be available and, until then, fossil power plants may become obsolete. Thus, we expect that medium scale systems will first be developed for useful applications. In particular, off-grid applications in regions where the climate does not permit the use of photovoltaic systems justifies the still high effort required for novel systems. We expect that geothermal energy may be the first explored source as it supports a quite constant temperature difference. For miniaturized systems the most promising applications are sensor applications and wearables, since thermomagnetic systems avoid the effort required for wiring or the service required to replace batteries.

Data availability statement

The data generated and/or analysed during the current study are not publicly available for legal/ethical reasons but are available from the corresponding author on reasonable request.

ORCID iD

Sebastian Fähler https://orcid.org/0000-0001-9450-4952

References

[1] Silvy Y, Guilyardi E, Sallée J-B and Durack P J 2020 Human-induced changes to the global ocean water masses and their time of emergence *Nat. Clim. Change* **10** 1030–6
[2] Tokarska K B, Hegerl G C, Schurer A P, Ribes A and Fasullo J T 2019 Quantifying human contributions to past and future ocean warming and thermosteric sea level rise *Environ. Res. Lett.* **14** 074020
[3] Schierning G 2018 Bring on the heat *Nat. Energy* **3** 92–93
[4] Champier D 2017 Thermoelectric generators: a review of applications *Energy Convers. Manage.* **140** 167–81

[5] Christiaanse T and Brück E 2013 Proof-of-concept static thermomagnetic generator experimental device *Metall. Mater. Trans.* E **1** 36–40
[6] Kishore R A and Priya S 2018 A review on design and performance of thermomagnetic devices *Renew. Sustain. Energy Rev.* **81** 33–44
[7] Brillouin L and Iskenderian H 1948 Thermomagnetic generator *Electr. Commun.* **25** 300–11
[8] Dzekan D, Waske A, Nielsch K and Fähler S 2021 Efficient and affordable thermomagnetic materials for harvesting low grade waste heat *APL Mater.* **9** 011105
[9] Tesla N 1890 *US Patent* 428057A
[10] Edison T A 1892 *US Patent* 476983A
[11] Srivastava V, Song Y, Bhatti K and James R D 2011 The direct conversion of heat to electricity using multiferroic alloys *Adv. Energy Mater.* **1** 97–104
[12] Pecharsky V K and Gschneidner K A Jr 1997 Giant magnetocaloric effect in $Gd_5(Si_2Ge_2)$ *Phys. Rev. Lett.* **78** 4494–7
[13] Waske A, Gruner M E, Gottschall T and Gutfleisch O 2018 Magnetocaloric materials for refrigeration near room temperature *MRS Bull.* **43** 269–73
[14] Waske A, Dzekan D, Sellschopp K, Berger D, Storck A, Nielsch K and Fähler S 2019 Energy harvesting near room temperature using a thermomagnetic generator with a pretzel-like magnetic flux topology *Nat. Energy* **4** 68–74
[15] Almanza M, Pasko A, Mazaleyrat F and LoBue M 2017 First- versus second-order magnetocaloric material for thermomagnetic energy conversion *IEEE Trans. Magn.* **53** 2502106
[16] Ghosh S, Ghosh A, Sen P and Mandal K 2020 Giant room-temperature magnetocaloric effect across the magnetostructural transition in $(Mn\,Ni\,Si)_{1-x}(Fe\,Co\,Ga)_x$ alloys *Phys. Rev. Appl.* **14** 014016
[17] Ahmad A, Mitra S, Srivastava S K and Das A K 2021 Giant magnetocaloric effect in Co_2FeAl Heusler alloy nanoparticles *J. Appl. Phys.* **54** 385001
[18] Ahmad A, Mitra S, Srivastava S and Das A 2021 Structural, magnetic and magnetocaloric properties of Fe_2CoAl Heusler nanoalloy *J. Magn. Magn. Mater.* **540** 168449
[19] Ma Z *et al* 2021 Thermomagnetic generation performance of Gd and $La(Fe,Si)_{13}H_y$/In material for low-grade waste heat recovery *Adv. Sustain. Syst.* **5** 2000234
[20] Dzekan D, Diestel A, Berger D, Nielsch K and Fähler S 2021 Can gadolinium compete with La–Fe–Co–Si in a thermomagnetic generator? *Sci. Technol. Adv. Mater.* **22** 643–57
[21] Swiss Blue Energy AG 2018 Der neue geniale beitrag zum energiewandel (available at: www.swiss-blue-energy.ch/en/index.html)
[22] Ahmed R, Kim Y, Mehmood M U, Shaislamov Z, U and Chun W 2019 Power generation by a thermomagnetic engine by hybrid operation of an electromagnetic generator and a triboelectric nanogenerator *Int. J. Energy Res.* **43** 5852–63
[23] Kishore R A, Singh D, Sriramdas R, Garcia A J, Sanghadasa M and Priya S 2020 Linear thermomagnetic energy harvester for low-grade thermal energy harvesting *J. Appl. Phys.* **127** 044501
[24] Ahmed Z, R, Mehmood M U, Kim Y, Lee J and Chun W 2020 Harnessing low-grade waste heat by operating a hybrid piezoelectric-electromagnetic energy harvester combined with a thermomagnetic engine *Int. J. Energy Res.* **44** 10710–23
[25] Gottschall T, Skokov K P, Fries M, Taubel A, Radulov I, Scheibel F, Benke D, Riegg S and Gutfleisch O 2019 Making a cool choice: the materials library of magnetic refrigeration *Adv. Energy Mater.* **9** 1901322
[26] Dan'kov S Y, Tishin A M, Pecharsky V K and Gschneidner K A 1998 Magnetic phase transitions and the magnetothermal properties of gadolinium *Phys. Rev.* B **57** 3478–90